The Mast Cell Function-Associated Antigen and Its Interactions with the Type I Fcε Receptor†

Jinming Song,‡ Guy M. Hagen,‡ Deborah A. Roess,‡ Israel Pecht,§ and B. George Barisas*,‡

Department of Chemistry, Colorado State University, Fort Collins, Colorado 80523, and Department of Immunology, The Weizmann Institute of Science, 76100 Rehovot, Israel

Received July 27, 2001

ABSTRACT: Rat mucosal-type mast cells of the RBL-2H3 line express a glycoprotein termed the MAst cell Function-associated Antigen (MAFA). When MAFA is clustered by its specific monoclonal antibody G63, secretion normally triggered by aggregating these cells' type I Fcε receptor (FcεRI) is substantially inhibited. The nature of MAFA−FcεRI interactions giving rise to this inhibition remains unclear. Rotational diffusion of a membrane protein is a sensitive probe of its involvement in intermolecular interactions. We have therefore studied by time-resolved phosphorescence anisotropy the rotational behavior of both MAFA and FcεRI as ligated by various reagents involved in FcεRI-induced degranulation and MAFA-mediated inhibition thereof. From 4 to 37 °C, the rotational correlation times (mean ± SD) of FcεRI-bound, erythrosin-conjugated IgE resemble those observed for MAFA-bound, erythrosin-conjugated G63 Fab, 82 ± 17 and 79 ± 31 μs at 4 °C, respectively. Clustering the FcεRI−IgE complex by antigen or by anti-IgE increases the phosphorescence anisotropy of G63 Fab and slows its rotational relaxation. Lateral diffusion of G63 Fab is also slowed by antigen clustering of the receptor. Taken together, these results indicate that unperturbed MAFA associates with clustered FcεRI. They are also *consistent* with its interaction with the isolated receptor.

One group of immunoreceptors, the Fc receptors, are specific for the respective Fc domains of immunoglobulin isotypes and bind them with a stoichiometry of 1:1. Binding by itself does not initiate degranulation of the cells; *clustering* of Fc receptors via the bound immunoglobulins which serve as antigen-specific, divalent adapters provides the signal leading to the above cellular response (*1*). Mast cells are an important experimental system for studying the events coupling Fc receptors to cellular responses. These cells respond instantly to clustering of their type I Fcε receptors (FcεRI)[1] by secreting their granules' contents, a process which can be quantitatively monitored (*2, 3*). The commonly employed and stable rat mucosal-type RBL-2H3 mast cell line has (3−6) × 10^5 FcεRI per cell, and these bind IgE with nanomolar affinity (*4*). Clustering the FcεRI initiates a cascade of biochemical processes leading to secretion of granule-stored mediators such as histamine (*5*) and the de novo synthesis and secretion of arachidonic acid metabolites (*6*) and of several cytokines (*7, 8*). The coupling cascade includes recruitment and activation of specific protein tyrosine kinases (*9*). This in turn causes a transient increase in tyrosine phosphorylation of several cellular proteins (*10, 11*). Resulting activation of PLCγ increases phosphatidylinositide hydrolysis (*12*) and, in turn, elevates intracellular free calcium ion concentrations and activates protein kinase C (*13*), finally culminating in the secretory response.

Several membrane proteins are capable of modulating the FcεRI-mediated secretory response (*14*−*18*). One such is a membrane glycoprotein named MAst cell Function-associated Antigen or MAFA. Pecht and co-workers identified MAFA as the target of the mAb G63 which inhibits RBL-2H3 cell degranulation induced by FcεRI clustering. Although at most 1 MAFA is expressed for every 10 FcεRI, clustering MAFA using the specific mAb G63 inhibits by up to 80% the secretory response of 2H3 cells to subsequent FcεRI clustering (*19*). The question of how such a protein, expressed in substoichiometric amounts, can deliver negative signals overriding those of the aggregated FcεRI is difficult to answer. MAFA aggregation inhibits the FcεRI-induced signaling cascade upstream of PLCγ activation, namely, suppressing both phosphatidylinositide phosphate hydrolysis and transient intracellular calcium elevation (*19, 20*). The inhibitory effect of mAb G63 requires MAFA clustering and is not due to interference with IgE−FcεRI interactions (*19*).

MAFA has been shown to be a glycoprotein with a molecular mass of 28−40 kDa when expressed as a monomer and to also exist as a disulfide-linked homodimer (*20*). Expression cloning of the cDNA encoding the MAFA has

† This work was supported in part by United States−Israel Binational Science Foundation Grant 96-00445 to I.P. and B.G.B., by NIH Grant HD33236 to D.A.R., and by NSF Grant MCB-9807822 to B.G.B.

* To whom correspondence should be addressed at the Department of Chemistry, Colorado State University, Fort Collins, CO 80523. Tel: 970-491-6641; Fax: 970-491-1801; Email: barisas@lamar.colostate.edu.

‡ Colorado State University.

§ The Weizmann Institute of Science.

[1] Abbreviations: 2H3 cell, rat mucosal mast cell of the RBL-2H3 line; BCR, B cell receptor; Er, erythrosin isothiocyanate; FcεRI, type I (high affinity) Fcε receptor; FPR, fluorescence photobleaching recovery; FRET, fluorescence resonant energy transfer; ITAM, immunoreceptor tyrosine-based activation motif; ITIM, immunoreceptor tyrosine-based inhibitory motif; mAb, monoclonal antibody; MAFA, mast cell function-associated antigen; PBS, phosphate-buffered saline; TPA, time-resolved phosphorescence anisotropy.

10.1021/bi011566i CCC: $22.00
Published on Web 12/22/2001

shown that it contains a single open reading frame, encoding a 188 amino acid long, type II integral membrane glycoprotein (*21*). The deduced 114 amino acid C-terminal (extracellular) domain displays a marked homology with the carbohydrate binding domain of calcium-dependent animal lectins including the type II FcεRI (CD23) and the natural killer cell receptors. More recently, it was indeed shown to bind terminal mannose residues (*22*). MAFA's 34 amino acid cytoplasmic tail contains an SIYSTL motif, an analogue of the immunoreceptor tyrosine-based inhibitory motif (ITIM) (*21*). The tyrosyl residue of the MAFA's ITIM is at least partly phosphorylated upon its clustering (*21, 23*).

MAFA−FcεRI Interactions: Hypothesis and Rationale for Experimentation. Previous studies in other laboratories and ours suggest certain parameters of interactions between FcεRI and MAFA, the membrane localization of these species, and the linkage of these interactions to the aggregation state of the molecular species.

1. Unperturbed, nonaggregated FcεRI are dispersed within the plasma membrane (*24*) but, upon aggregation, are translocated into lipid rafts as has been shown by Baird's group (*25*).

2. The Jovin laboratory has provided the crucial demonstration of FRET between FcεRI-bound IgE and MAFA-bound intact G63 mAb and shown that this energy transfer is *not* increased upon FcεRI clustering (*26*). Unfortunately, in this study, receptor interactions with *unclustered* MAFA, as probed by G63Fab, were not examined.

3. Evidence for MAFA−FcεRI association was implied by 2H3 cell degranulation apparently being triggered by bifunctional antibodies specific for FcεRI and MAFA (*27*). Data analysis in this paper is based on the assumption that only aggregation of FcεRI can cause cell degranulation, whereas MAFA−FcεRI clusters are considered as inactive. In such a case, the degranulation caused by bifunctional antibodies can only be explained by invoking preexisting MAFA−FcεRI aggregates.

These results leave certain questions unresolved. In particular, there is no *direct* experimental evidence for the interaction of *unclustered* MAFA with FcεRI. Specifically, is MAFA, in the *absence* of bridging ligands such as mAb G63, associated with isolated FcεRI? Is it associated with clustered FcεRI?

We may hypothesize, reasoning from the above FRET and bifunctional antibody results, that MAFA is at least partly associated with the FcεRI, irrespective of the latter's aggregation state. Such a circumstance could be tested by measuring the in-membrane motions of MAFA and the receptor. Such measurements have the advantage of being performed on intact cells under nearly physiological conditions. Rotational behavior of membrane proteins, measured by time-resolved phosphorescence anisotropy (TPA), is a sensitive reflection of molecular size since the rotational correlation time (RCT) of anisotropy decay is linearly proportional to the molecule's in-membrane volume (*28*). The lateral diffusion coefficient, or diffusion constant, of membrane proteins measured by fluorescence photobleaching recovery (FPR) is a weaker, i.e., logarithmic, function of molecular size (*28*). Therefore, if MAFA is constitutively associated with the FcεRI, then TPA and FPR measurements on the MAFA−FcεRI system should yield certain specific results, given that the receptor is present in large excess.

1. MAFA should exhibit the same apparent rotational correlation time as the FcεRI, and this value should be too large for an isolated molecule of MAFA's size.

2. Aggregating the receptor into large clusters should reduce the lateral diffusion coefficients of both MAFA and the receptor.

3. Such treatment should rotationally immobilize both MAFA and the receptor, thus increasing the limiting anisotropies of both species.

We have thus performed TPA and FPR measurements to resolve the nature of interactions between FcεRI and MAFA.

MATERIALS AND METHODS

Antibodies and Proteins. mAb G63 (IgG_1) used in the present studies was purified from hybridoma culture supernatants by chromatography on protein A−Sepharose. The mAb was eluted from the column by 0.2 M sodium citrate (pH 4.5) and collected directly in tubes containing 2 M Tris buffer (pH 8.2). The mAb was dialyzed against phosphate-buffered saline (1.86 mM NaH_2PO_4, 8.39 mM Na_2HPO_4, 0.15 M NaCl, pH 7.4; PBS) and stored frozen at −20 °C. Fab fragments of mAb G63 were prepared by digestion with papain at a 1:50 w/w ratio, in 20 mM Tris buffer (pH 8.2), containing 0.1 mM dithiothreitol and 2 mM EDTA. Digestion was carried out for 2 h at 37 °C, after which time iodoacetamide (10 mM) was added for 1 h at 4 °C. Fc fragments and undigested antibodies were eliminated by passing the preparations twice through the protein A−Sepharose column. SDS−PAGE followed by Coomassie blue staining was used to verify that Fab preparations did not contain intact or partially digested molecules. Antibody concentrations were determined by absorbance at 280 nm. G63-$F(ab')_2$ was prepared by pepsin (2.4% w/w) digestion of intact G63 (1.35 mg/mL) in 0.1 M sodium citrate, pH 3.7, at 37 °C for 2 h. The reaction was stopped by increasing the pH to 7.0. The $F(ab')_2$ product was purified by chromatography on MAPS II Protein A agarose with the MAPS II binding buffer or on HiTrap Protein G columns. Monoclonal DNP-specific A2 rat IgE was purified from ascitic fluid by binding to DNP-Sepharose and elution with DNP-glycine (*4*). 95.3 anti-mouse IgE was purified as previously described (*29*). Goat anti-mouse IgG (Fab-specific; M6898), rabbit anti-mouse IgG (M7023), goat anti-mouse IgG (Fc-specific; M2650), and goat anti-DNP IgG (D9781) antibodies were obtained from Sigma, St. Louis, MO. DNP_{11}-BSA, derivatized with an average of 11 DNP groups per molecule, was prepared as described earlier (*30*).

Preparation of Antibody Conjugates. Antibodies were derivatized with erythrosin isothiocyanate (Er; Molecular Probes, Eugene, OR) using a modification of methods described by Johnson and Holborow (*31*). Intact antibody or Fab or $F(ab')_2$ fragments were dissolved in PBS containing 50 mM sodium borate, pH 9.3. Er was dissolved in 50 μL of DMSO and diluted with 50 mM sodium borate buffer. Er concentrations were determined spectrophotometrically at 535 nm using a molar absorptivity of 101 000 L mol^{-1} cm^{-1}. A 3-fold molar excess of Er was added to the protein solutions, and the mixtures were incubated at room temperature for 2 h. The reaction was quenched with 1 M Tris, and dye-derivatized proteins were separated from free dye on a Sephadex G25 column. The column eluate was extracted

once with an equal volume of 1-butanol to remove any remaining noncovalently bound dye and dialyzed against PBS for a total of 48 h at 4 °C. The molar ratios for dye-derivatized proteins and their concentration in solution were determined spectrophotometrically. The antibody preparations used in these experiments had an average of 1−2 mol of Er/mol of intact antibody, Fab, or F(ab′)$_2$ fragments. Monofunctional Cy3 and Alexa 488 were purchased from Amersham Pharmacia Biotech (Piscataway, NJ) and Molecular Probes (Eugene, OR), respectively, and used for antibody derivatization according to the manufacturers' directions. Prior to use, all dye-derivatized proteins were centrifuged at 130000*g* for 10 min in a Beckman Airfuge (Beckman Instruments, Palo Alto, CA) to remove any protein aggregates formed during storage.

RBL-2H3 Cells. Rat mucosal-type mast cells of the RBL-2H3 line were kindly provided by Dr. Reuben Siraganian of the National Institutes of Health. Cells were grown as monolayers in Eagle's minimal essential medium with Earle's salts (MEM) supplemented with 10% fetal calf serum, 2 mM glutamine, and antibiotics in a humidified atmosphere with 5% CO_2 at 37 °C. Cells labeled with FITC-IgE and compared cytometrically with calibrated fluorescein bead standards showed typical expression of 290 000−400 000 FcεRI per cell (*32*). Typically, 10^7 cells in 1 mL were labeled with Er-derivatized probe for each TPA experiment. Cell labeling conditions for fluorescent or phosphorescent protein conjugates were 150 nM IgE or 30 nM G63 mAb, Fab, or (Fab′)$_2$ at 4 °C for 1 h. Following this, cells were washed twice by centrifugation at 300*g* for 3 min in PBS to remove unbound ligand and were deoxygenated to eliminate phosphorescence quenching by O_2. To accomplish this, pelleted cells were resuspended in deaerated PBS containing 50 mM D-glucose, 0.2 mg/mL glucose oxidase (Sigma type II-S), and 0.25 mg/mL catalase (Sigma type C-10) (*33*). The sample was incubated for 5 min before the cells were pelleted and gently resuspended in 0.5 mL of supernatant, followed by argon purging for 15 min before measurements.

Phosphorescence measurements of MAFA-bound erythrosin-G63 mAb and its Fab fragment require particular care in cell labeling. Although G63 binds MAFA with good affinity, 1×10^8 M^{-1} for the Fab fragment (*4*), the low expression of MAFA means that particular care must be taken in selecting labeling conditions in order to attain maximum specific binding. We measured phosphorescence signals achieved by specific and nonspecific binding of mAb G63 to MAFA at various antibody concentrations. The data show that only in a narrow range of antibody concentrations is an adequate signal attributable to specific binding attained. A 30 nM concentration provided approximately 90% specific binding and a reasonable signal. This labeling concentration was used for all experiments involving intact G63 mAb or its Fab or F(ab′)$_2$ fragments. Under these conditions, phosphorescence signals from G63 Fab-labeled cells were at least 10-fold above the background signal from unlabeled cells.

Time-Resolved Phosphorescence Anisotropy Instrumentation and Analysis. Time-resolved phosphorescence anisotropy experiments were performed as previously described (*34*, *35*), and the latter reference provides a block diagram of the apparatus employed. Washed and deoxygenated cell samples were placed in a 5 × 5 mm Suprasil quartz cuvette mounted in a thermostated housing, typically maintained at 4 °C unless otherwise specified. Excitation was by the frequency-doubled 532 nm output of a Spectra-Physics DCR-11 Nd:YAG laser operated at 10 Hz with a vertically polarized TEM 00 output of 250 μJ at the sample cuvette. Sample phosphorescence was isolated by a holographic notch filter (Kaiser Optical), a 1 M $Na_2Cr_2O_7$ solution chemical filter, a KV 550 color filter (Schott Glass Technologies, Inc., Duryea, PA) to block scattered light, a 3 mm thick RG 665 filter to eliminate delayed fluorescence, and a rotating polarizer to select phosphorescence emitted with vertical $I_{||}(t)$ and horizontal $I_{\perp}(t)$ polarizations. The phosphorescence signal was detected by a thermoelectrically cooled EMI 9816 photomultiplier tube protected from light scattered during laser pulses by a fast gating circuit (*36*). The photomultiplier output was amplified by a Tektronix 476 oscilloscope and a 35 MHz bandwidth buffer amplifier, and 4096 traces in each polarizer orientation were averaged by a Nicolet 12/70 computer equipped with a 20 MHz, 8-bit ADC. Data were downloaded into a PC-compatible computer for analysis. Phosphorescence intensities, $I_{||}(t)$ and $I_{\perp}(t)$, were analyzed (*37*) to yield a phosphorescence intensity function, $s(t) = I_{||}(t) + 2I_{\perp}(t)$, and a phosphorescence anisotropy function, $r(t) = [I_{||}(t) - I_{\perp}(t)]/s(t)$. The phosphorescence intensity function was fitted to a sum of six fixed exponential decays of 3, 10, 30, 100, 300, and 1000 μs, respectively. To facilitate comparison of phosphorescence decay between samples, mean decay half-times were calculated from the lifetimes and amplitudes of each step. Results of the lifetime analysis were used to weigh points in a nonlinear least-squares fit of the anisotropy data. Anisotropy data were thus satisfactorily analyzed according to a single average exponential decay model: $r(t) = r_\infty + (r_0 - r_\infty) \exp(-t/\varphi)$, which yielded the initial anisotropy value r_0, the limiting anisotropy value r_∞, and the rotational correlation time φ as well as the statistical uncertainties in these quantities (*38*).

Erythrosin-conjugated antibodies bound to cell membrane proteins typically exhibit initial anisotropies of 0.04−0.08. These values thus reflect considerable randomization of chromophore orientation on the sub-microsecond time scale. Anisotropy is observed to decay exponentially from its initial value r_0 to a final value r_∞, the time constant being the rotational correlation time φ, a quantity proportional to the in-membrane volume of the labeled protein and sensitive enough to reveal receptor dimerization events (*39*). The limiting anisotropy value r_∞, as observed at long times, arises from restrictions to free rotation of the labeled molecule. It is therefore common to speak of r_∞ as reflecting a rotationally immobile fraction and such rotational immobilization of molecules effectively occurs whenever a protein joins an aggregate which is some 10 or more times its size. All membrane proteins also exhibit some intrinsic limiting anisotropy since they rotate uniaxially rather than freely in three dimensions.

Differences in r_0 and r_∞ values between nontreated and treated cells were compared by Student's *t*-test (*40*) as implemented for equal sample numbers (*41*) to evaluate the probabilities that the rotational parameters observed in untreated and control samples could have arisen by sampling a single population, i.e., in the absence of an effect of treatment on probe rotation. The probability of observing differences between treated and control samples in two or

Table 1: Comparison of Rotational Parameters of FcεRI-Bound Erythrosin-IgE and MAFA-Bound Erythrosin-G63 Fab at 4 °C[a]

						decay fractions[f]						
species	RCT (μs)[b]	r_0[c]	r_∞[d]	intensity[e]	3	10	30	100	300	1000	$t_{1/2}$ (μs)[g]	n[h]
IgE	82 ± 17	0.068 ± 0.010	0.039 ± 0.010	1.6×10^6	0.09	0.16	0.16	0.17	0.38	0.03	44 ± 10	23
G63 Fab	79 ± 31	0.061 ± 0.022	0.047 ± 0.015	0.3×10^6	0.22	0.33	0.18	0.12	0.12	0.03	16 ± 2	21

[a] All indicated uncertainties are standard deviations of independent replicate measurements. [b] Rotational correlation time in microseconds. [c] Initial phosphorescence anisotropy. [d] Limiting, i.e., infinite-time, phosphorescence anisotropy. [e] Relative phosphorescence intensity. [f] Fractional phosphorescence decay amplitudes for the indicated time constants (μs). The typical standard deviation of individual fractions is about 0.02. [g] Half-time for phosphorescence decay evaluated from the fitted decay curve. [h] Number of samples examined.

more treatment groups when no treatment actually has effect is simply the product of probabilities for observing the individual effects. Rotational correlation times were not compared in this way. Many of the rotational correlation times reported in this study contain quite large relative errors, yet all such distributions are bounded on the left by zero. Such distributions are thus intrinsically skewed to the right, i.e., in the direction of larger values, and so cannot be considered normal for statistical analysis.

Fluorescence Photobleaching Recovery Instrumentation and Analysis. Equipment and methods for FPR measurements have been published elsewhere in detail (*42*). The interference fringe technique provides extraordinarily high sensitivity for measurements on sparsely expressed membrane proteins such as MAFA though determination of protein mobile fractions is somewhat more sensitive to factors such as cellular autofluorescence. The microscope photometer is based on the Zeiss Axiomat microscope equipped with a Zeiss 63×, NA 1.2, Plan Neofluar immersion fluorescence objective, a fluorescence vertical illuminator, and an MP03 photometer module. Standard Zeiss filters for fluorescein and tetramethylrhodamine were used with Omega dichroic mirrors 510DRLPO2 and 540DRLPO2 for measurements involving Alexa 488 and Cy3, respectively. Measurements were performed at 23 °C. A Coherent Radiation Innova 100 argon ion laser provided excitation at 488 nm for Alexa 488-conjugated proteins and at 514 nm for Cy3-conjugated proteins. The illuminated region had a $1/e^2$ radius of 17 μm with laser powers of 1.6 W in the bleaching pulse and 500 μW in the probe beam. An interferometer divided the laser beam into two equal intensity components separated by a center-to-center distance of 5.5 mm (*42*), giving a fringe spacing at the sample of 1.75 μm. Typical experiment run times were 15 s pre-bleach and 25 s post-bleach with 50 ms/point data acquisition and a bleaching time of 800 ms. Recovery traces obtained from unlabeled cells were subtracted from labeled cell traces to correct for cellular autofluorescence. The equations defining fluorescence recovery kinetics for spot photobleaching and for fringe photobleaching of spherical samples have already been presented elsewhere in detail (*42*). Unadjusted raw data were represented directly in terms of the various parameters associated with a given measurement including the pre-bleach and immediate post-bleach fluorescence levels, the percentage of fluorophores mobile on the time scale of the experiment, and an appropriate function representing the recovery kinetics in terms of a decay half-time. The parameters were evaluated directly by the Marquardt nonlinear least-squares procedure (*43*). From the measured time at which fluorescence recovery is half-complete and from the known optical parameters, the diffusion constant and the fraction of labeled molecules mobile on the experimental time scale were then evaluated.

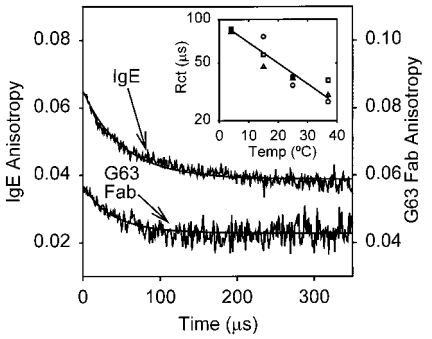

FIGURE 1: Anisotropy decay kinetics for Er-IgE and Er-G63 Fab bound to 2H3 cells at 4 °C. Traces shown are averages of 21 experiments (IgE) and 23 experiments (G63). The inset shows the temperature dependence of rotational correlation times for the above species as well as Er-G63 intact mAb. Symbols in inset graph: (○) IgE; (□) G63Fab; (△) G63 mAb. All points are satisfactorily fitted by a single curve with rotational correlation times of 84 μs at 4 °C and 28 μs at 37 °C. This corresponds to an activation energy of 5.9 kcal mol^{-1}, a value typical of diffusive flow in membranes.

RESULTS

FcεRI-Bound IgE and MAFA-Bound G-63 Fab Behave Similarly as Unconstrained Membrane Proteins in Time-Resolved Phosphorescence Anisotropy Experiments. A comparison of TPA measurement results for FcεRI-bound IgE and MAFA-bound G63 Fab at 4 °C is presented in Table 1 and Figure 1. Decay kinetics of the erythrosin phosphorescence intensity function are markedly multiexponential (Table 1). Analysis shows that the largest component of IgE phosphorescence decay is that at 300 μs, but that substantial amounts of all the other components contribute to the observed decay curves. The much lower signals observed for MAFA allow some contribution from phosphorescent components of cytoplasm, and this is manifested in the apparent shorter phosphorescence lifetimes observed for MAFA-bound G63 Fab probes. Nonetheless, the overall phosphorescence decay curves (data not shown) of cell-bound Er-IgE and Er-G63 Fab both appear very similar.

Parameters for anisotropy decay at 4 °C are also presented in Table 1. The rotational correlation times for FcεRI-bound IgE and for MAFA-bound G-63 Fab are virtually identical at 82 ± 17 μs (mean ± SD *not* SEM) and 79 ± 31 μs, respectively. Rotational correlation times also decrease with increasing temperature (Figure 1 inset). For IgE, this decrease is from 82 μs at 4 °C to 27 μs at 37 °C, i.e., about 3-fold over this temperature range. In contrast, the initial and limiting anisotropies change very little over this range. MAFA's rotational correlation time changes similarly, from 79 μs at 4 °C to 38 μs at 37 °C.

Table 2: Effect of Various Treatments on Rotation of FcεRI-Bound Erythrosin-Conjugated IgE at 4 °C[a]

	r_0[b]		r_∞[c]		RCT (μs)[d]		
treatment	treated	control	treated	control	treated	control	n[e]
DNP_{11}-BSA (1 μg/mL)[f]	0.087	0.068	0.058	0.037	96	75	1
DNP_{11}-BSA (10 μg/mL)[g]	0.102	0.064	0.073	0.036	93	85	1
anti-IgE[h]	0.078	0.067	0.036	0.033	85	85	1
anti-IgE+anti-IgG[i]	0.086	0.067	0.042	0.033	86	85	1
DNP_{11}-BSA+anti-IgE[j]	0.096	0.067	0.068	0.033	71	85	1
G63 Fab+anti-IgG (Fab-spec)[k]	0.070 ± 0.006	0.073 ± 0.005	0.056 ± 0.009	0.054 ± 0.012	127 ± 74	165 ± 83	4
G63 F(ab′)$_2$+anti-IgG (Fab-spec)[l]	0.078 ± 0.006	0.076 ± 0.009	0.063 ± 0.006	0.058 ± 0.007	108 ± 47	89 ± 16	7

[a] Parameters for treated and control samples were obtained in the same experiment. All indicated uncertainties are standard deviations of independent replicate measurements. [b] Initial phosphorescence anisotropy. [c] Limiting, i.e., infinite-time, phosphorescence anisotropy. [d] Rotational correlation time in microseconds. [e] Number of separate replicate measurements. [f] DNP_{11}-BSA 1 μg/mL for 30 min at 25 °C. [g] DNP_{11}-BSA 10 μg/mL for 30 min at 37 °C. [h] Anti-IgE 6 μg/mL for 30 min at 37 °C. [i] Anti-IgE 6 μg/mL for 30 min at 37 °C, then rabbit anti-mouse IgG 6 μg/mL for 30 min at 37 °C. [j] DNP_{11}-BSA 70 μg/mL for 60 min at 37 °C, then anti-IgE 6 μg/mL for 30 min at 37 °C. [k] G63 Fab 30 nM for 60 min at 4 °C, then 14 μg/mL goat anti-mouse IgG (Fab specific) for 30 min at 37 °C. [l] G63 F(ab′)$_2$ 30 nM for 1 h at 4 °C, then 14 μg/mL goat anti-mouse IgG (Fab specific) for 30 min at 37 °C.

Table 3: Effect of Various Treatments on Lateral Diffusion of FcεRI-Bound Cy3-Conjugated IgE and Alexa 488-Conjugated G63 Fab at 23 °C[a]

probe	treatment	D ($\times 10^{-10}$ cm^2 s^{-1})[b]	M (%)[c]	n
IgE	none	3.9 ± 0.5	71 ± 3	10
IgE	DNP_{11}-BSA[d]	2.8 ± 0.4	75 ± 3	10
IgE	G63 mAb[e]	3.7 ± 0.3	73 ± 1	10
G63 Fab	none	2.2 ± 0.5	36 ± 3	10
G63 Fab	DNP_{11}-BSA[d]	0.8 ± 0.5	36 ± 1	10
G63 Fab	anti-IgG+second Ab[f]	0.18 ± 0.04	38 ± 1	10

[a] Measurements performed using interference fringe fluorescence photobleaching recovery. All indicated uncertainties are standard deviations of independent replicate measurements. [b] Lateral diffusion coefficient. [c] Mobile fraction. [d] DNP_{11}-BSA 64 μg/mL for 30 min at 4 °C. [e] 30 nM G63 mAb for 1 h at 4 °C. [f] G63 Fab 30 nM for 1 h at 4 °C, goat anti-mouse IgG 14μg/mL for 1 h at 4 °C, and donkey anti-goat IgG 14 μg/mL for 1 h at 4 °C.

FcεRI Clustering by Multivalent Ligands Strongly Affects Its Membrane Dynamics. Polyvalent ligands such as antigen (DNP_{11}-BSA), which cluster the FcεRI−IgE complexes and which are thus effective in triggering mast cell degranulation, markedly affect the rotational motion of the FcεRI. For example, in one experiment, treatment with 1 μg/mL DNP_{11}-BSA for 30 min at 37 °C increased r_0 from 0.068 to 0.087, increased r_∞ from 0.037 to 0.058, and produced a small increase in RCT from 75 to 95 μs. Table 2 summarizes the effects of various treatments on FcεRI rotational dynamics. These effects were found to depend somewhat on antigen concentration when concentrations from 40 ng/mL to 70 μg/mL were used to cluster the FcεRI. Other FcεRI clustering reagents, and combinations thereof, were examined, but none were more effective than antigen in restricting receptor rotational motion. MAFA was aggregated on cells binding Er-IgE by either G63 Fab or G63 F(ab′)$_2$ followed in either case by a second antibody, Fab-specific polyclonal goat anti-mouse IgG. Er-IgE rotation was then measured. Neither of these treatments had a discernible effect on rotation of receptor-bound Er-IgE (Table 2).

In addition, lateral diffusion of Cy3-conjugated IgE bound to variously treated 2H3 cells was measured by interference fringe fluorescence photobleaching recovery (Table 3). Antigen treatment substantially restricted IgE lateral diffusion: The diffusion coefficient declined from (3.9 ± 0.5) × 10^{-10} cm^2 s^{-1} on untreated cells to (2.8 ± 0.4) × 10^{-10} cm^2 s^{-1} after DNP_{11}-BSA treatment. By contrast, IgE diffusion coefficients measured on MAFA-oligomerized cells were (3.7 ± 0.3) × 10^{-10} cm^2 s^{-1}, a value indistinguishable from that of untreated cells. Mobile fractions were also equivalent at 71 ± 3% and 73 ± 1%, respectively.

MAFA Exhibits Similar Rotational Behavior Whether Monitored by Bound Intact mAb G63 or by Its Fab Fragment. Inhibition of FcεRI-induced degranulation requires that MAFA be clustered, e.g., by intact mAb G63 or by its F(ab′)$_2$ fragment, and thus it might be expected that either reagent would aggregate MAFA into dimers. In such a case, rotation of intact G63 mAb-labeled MAFA would be appreciably slower than that of Fab-labeled MAFA. Comparison of rotational correlation times for MAFA binding Fab and mAb labels properly should include all measurements in the "control" column for each ligand. When this is done, the 30 independent measurements using labeled Fab yield an average rotational correlation time of 77 ± 28 μs while the 19 measurements using labeled mAb average 89 ± 44 μs. This is far from the factor of 2 that might be expected, but it suggests that the mAb aggregates MAFA to some extent. Moreover, both initial and limiting anisotropy values and rotational correlation times of mAb-labeled control samples resembled those of Fab-labeled samples treated with DNP_{11}-BSA. Rotational parameters of mAb-labeled samples were not greatly changed by DNP_{11}-BSA treatment.

MAFA Rotation and Lateral Diffusion Are Restricted by FcεRI Clustering. A fundamental question is whether MAFA, when not aggregated, is nonetheless associated with FcεRI. We therefore measured the rotational motions of MAFA binding G63 Fab before and after FcεRI aggregation by antigen or anti-IgE. Averages of several anisotropy decay traces for MAFA rotation on cells variously treated and probed with Er-conjugated G63 Fab are shown in Figure 2. These traces show that FcεRI clustering by DNP_{11}-BSA produces a substantial increase in the anisotropy of G63 Fab while aggregation of MAFA via G63 Fab and polyclonal anti-IgG produces a somewhat larger increase.

Moreover, data in Table 4 show that clustering FcεRI-IgE by DNP_{11}-BSA or by anti-IgE consistently increases the initial anisotropy, the limiting anisotropy, and the rotational correlation times of MAFA-bound G63 Fab. Owing to the low expression of MAFA, there are large uncertainties in

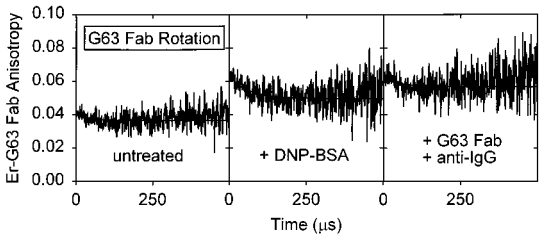

FIGURE 2: Effects of FcεRI and MAFA cross-linking on MAFA rotational diffusion at 4 °C as probed by Er-G63 Fab. Traces shown are averages of 3−6 independent measurements. The average rotational parameters from experiments such as that shown here are presented in Table 4. This table shows that FcεRI cross-linking by DNP_{11}-BSA and direct cross-linking of MAFA by G63 Fab and polyclonal anti-IgG increase the MAFA rotational correlation time from 79 μs to 110 and 151 μs, respectively. FcεRI cross-linking by DNP_{11}-BSA produces a small but consistent increase in the MAFA limiting anisotropy from 0.045 to 0.053 while direct MAFA cross-linking produces a larger increase in this quantity to 0.063. Both of these effects demonstrate restriction of MAFA rotation by either treatment.

these results, and thus questions may arise as to their statistical significance. However, as statistical analysis shows (cf. Materials and Methods), the likelihood that *all* effects on r_0 *and* r_∞ caused by DNP_{11}-BSA *and* anti-IgE treatments could have arisen accidentally is only about 1%. This strongly suggests that MAFA associates with clustered FcεRI even in the absence of MAFA clustering.

An effect of FcεRI aggregation on MAFA lateral diffusion was also observed. Clustering FcεRI by DNP_{11}-BSA reduced MAFA's diffusion coefficient from $(2.2 \pm 0.5) \times 10^{-10}$ cm^2 s^{-1} on untreated cells to $(0.8 \pm 0.5) \times 10^{-10}$ cm^2 s^{-1} after treatment. Figure 3 shows the visible slowing of MAFA fluorescence recovery after photobleaching on FcεRI-clustered cells. As would be expected, aggregating MAFA through G63Fab and anti-IgG produced a much larger effect on the MAFA diffusion coefficient, reducing it almost 10-fold to $(0.18 \pm 0.04) \times 10^{-10}$ cm^2 s^{-1}. Rotation of MAFA-bound intact mAb G63 also responds to FcεRI clustering, though this is less than for the corresponding MAFA-bound Fab (Table 4). In general, anti-IgE has larger effects on rotational parameters of mAb G63 than DNP_{11}-BSA.

The Fcγ Domain of mAb G63 Apparently Interacts with Additional 2H3 Cell Surface Receptors. G63 inhibition of 2H3 cell degranulation was originally discovered as an effect of cell treatment with the intact mAb (*4*). Although clustering G63 Fab was also shown to cause inhibition, we wondered nonetheless whether the Fcγ domain of this IgG_1-class antibody might also be involved in cell surface interaction, since 2H3 cells also express Fcγ receptors. We explicitly compared rotation of MAFA-bound erythrosin-G63 mAb and -G63 $F(ab')_2$ (Table 4). Three independent experiments show intact mAb G63 to exhibit higher anisotropies and a slower rotational correlation times than its $F(ab')_2$ derivative. Once again, differences are not large, but statistical analysis shows only an approximately 1% probability that both samples rotate equivalently. Moreover, differences in the rotational correlation time of the $F(ab')_2$ fragment and the intact mAb strongly suggest interaction of intact G63's Fcγ domain with a membrane entity such as FcγRII (CD32) (*44*).

DISCUSSION

A major issue pursued in this study is whether MAFA associates with FcεRI on nonperturbed cells. If most MAFA molecules are so associated, then they must exhibit the rotational correlation time of the unliganded FcεRI. We have therefore invested considerable effort in comparing the rotational parameters of FcεRI-bound IgE and MAFA-bound G63 Fab. Rotation of 2H3 cell bound IgE has been studied on several instances (*32*, *39*, *45*−*47*), and, for example, Zidovetzki et al. reported values in reasonable agreement with ours. There is much less information on MAFA rotational behavior (*32*, *48*). We also found that rotational correlation times are quite consistent for each protein at a given temperature, though anisotropy values, both initial and limiting, depend somewhat upon the batch of erythrosin conjugate employed. Thus, based on our current extensive measurements, we conclude that, while it is difficult to determine *precisely* how closely nonclustered IgE and MAFA rotational correlation times and anisotropies resemble each other, the differences, if any, seem slight.

The temperature dependence of FcεRI-bound IgE rotation has also been reported: Rotational correlation times typically fall about 3-fold as the temperature is increased from 4 to 37 °C (*32*, *45*). This is the same temperature dependence observed now both for FcεRI -bound IgE and for MAFA-bound G63 Fab (Figure 1 inset). A 3-fold increase in rotation rate over this temperature range corresponds to an activation energy of 5.9 kcal mol^{-1}, a value typical for diffusive processes in membranes and one that suggests that both FcεRI and MAFA move freely in the plasma membrane, either as independent species or with MAFA associated with a fraction of the FcεRI. One can summarize that the temperature dependence of unclustered MAFA's rotational parameters, within the considerable uncertainty of measurements on this weakly expressed species, also appears similar to those of nonperturbed FcεRI.

The rotation of FcεRI is consistent with that expected for a seven-transmembrane segment protein. Peters and Cherry estimated a hydrodynamic diameter of 4.3 ± 0.5 nm for bacteriorhodopsin (*49*), and this agrees reasonably well with the crystal structure recently published for bovine rhodopsin (*50*). If one combines this value with a membrane thickness of 6.5 nm, a typical membrane viscosity of 2 P at 37 °C, and an activation energy for viscous flow of 6 kcal mol^{-1}, a rotational correlation time of about 60 μs at 4 °C would be expected for a structure consisting only of the receptor's transmembrane domains. Similar calculations show that, owing to the much lower viscosity of the extracellular environment, the FcεRI extracellular domain should have essentially no effect on receptor rotation. Thus, this 60 μs value is to be compared with rotational correlation times of 82 μs measured at 4 °C for FcεRI and stands in quite good agreement with them. The rotational correlation time to be expected for MAFA depends on whether the monomer or the disulfide-linked dimer is the prevalent form. MHC class II molecules are similar in size to the MAFA dimer and contain two transmembrane segments. Thus, MAFA dimer rotation might be expected to resemble that of class II molecules. Rotational correlation times averaging 10 μs at 4 °C have been measured for a number of wild-type and cytoplasmically truncated I-A^k species (*51*) with somewhat

Table 4: Effect of Various Treatments on Rotation of MAFA-Bound Erythrosin-Conjugated G63 Fab and -mAb and $(Fab')_2$ at 4 °C[a]

			r_0[b]			r_∞[c]			RCT (μs)[d]	
probe	treatment	*n*	treated	control	prob[e]	treated	control	prob[e]	treated	control
G63 Fab	untreated	21	−	0.061 ± 0.022		−	0.047 ± 0.015		−	79 ± 31
	DNP_{11}-BSA[f]	6	0.067 ± 0.019	0.058 ± 0.024	0.25	0.052 ± 0.011	0.045 ± 0.014	0.17	110 ± 36	73 ± 22
	anti-IgE[g]	3	0.070 ± 0.013	0.057 ± 0.027	0.25	0.063 ± 0.017	0.046 ± 0.017	0.14	151 ± 129	76 ± 22
G63 mAb	untreated	12	−	0.060 ± 0.009		−	0.051 ± 0.008		−	82 ± 24
	DNP_{11}-BSA[f]	3	0.062 ± 0.005	0.063 ± 0.009	0.45	0.051 ± 0.004	0.053 ± 0.005	0.30	93 ± 17	98 ± 76
	anti-IgE[g]	4	0.072 ± 0.004	0.062 ± 0.009	0.05	0.062 ± 0.004	0.053 ± 0.005	0.02	110 ± 75	101 ± 58
G63 $F(ab')_2$	(vs G63 mAb)	3	0.061 ± 0.009	0.065 ± 0.007	0.30	0.044 ± 0.006	0.054 ± 0.005	0.03	49 ± 6	80 ± 14

[a] Parameters for G63 Fab reflect representative, comparably handled treated and control samples examined in the same experiment. For G63 mAb, untreated samples were examined as controls, treated as indicated, and remeasured. All indicated uncertainties are standard deviations of independent replicate measurements. [b] Initial phosphorescence anisotropy. [c] Limiting, i.e., infinite-time, phosphorescence anisotropy. [d] Rotational correlation time in microseconds. [e] Probability that treated and control results could have been observed from within a single population. [f] DNP_{11}-BSA 1−14 μg/mL for 30 min at 37 °C. [g] Anti-IgE 6 μg/mL for 30 min at 37 °C.

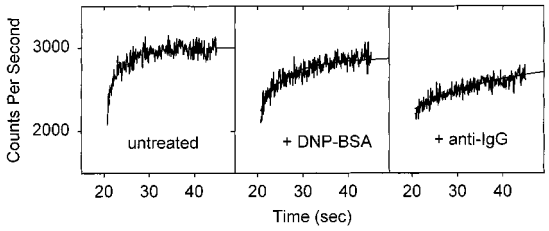

FIGURE 3: Effects of FcεRI and MAFA cross-linking on MAFA lateral diffusion at 23 °C as probed by Alexa 488-G63 Fab. Fluorescence recovery traces shown are from a single experiment, each representing an average of 10 individual cell measurements. The *y*-axes of the middle and right panels have been adjusted vertically to align recovery traces. Cross-linking FcεRI by DNP_{11}-BSA reduced MAFA's diffusion coefficient from $(1.90 \pm 0.24) \times 10^{-10}$ cm^2 s^{-1} on untreated cells to $(0.76 \pm 0.23) \times 10^{-10}$ cm^2 s^{-1} after DNP_{11}-BSA treatment. As would be expected, cross-linking MAFA through G63Fab and anti-IgG produced a much larger effect on the MAFA diffusion coefficient, reducing it almost 10-fold to $(0.19 \pm 0.03) \times 10^{-10}$ cm^2 s^{-1}.

slower rotation measured for I-A^d (*34*). Hence, the rotational correlation times of FcεRI and MAFA dimers would be *expected* to differ substantially (60−80 μs vis à vis 10−20 μs) with a correspondingly larger difference expected for monomeric MAFA molecules. By contrast, the rotational correlation times of unperturbed FcεRI-bound IgE and MAFA-bound G63 Fab are indistinguishable (82 and 79 μs, respectively). Intrinsic association of MAFA with FcεRI is thus consistent with these results.

Clustering of FcεRI by multivalent ligand, whether by IgE and antigen or by polyclonal anti-IgE, markedly restricts the receptor's rotational and lateral motion. Large receptor aggregates are formed and, as Baird et al. have shown (*52*), translocated to lipid rafts. The rotational correlation time of spherical objects depends linearly upon their molecular mass (*53*), and for asymmetrical objects, the dependence on size is much stronger. Large FcεRI aggregates formed by multivalent ligands thus appear immobile in microsecond time scale rotation experiments. Such aggregation, which can also be produced by chemical cross-linking, therefore increases both the initial and limiting anisotropies of the aggregated protein (*34*). However, large aggregate formation is limited kinetically by the lateral diffusion of smaller aggregates. As aggregation proceeds, both the diffusion coefficients and the concentrations of aggregates decrease so that equilibrium is never actually attained (*54*). The specific rotational parameters observed are therefore functions of incubation time and temperature and ligand concentration and valence. In our experiments, DNP_{11}-BSA treatment of FcεRI binding the DNP-specific monoclonal IgE increases both the initial and the limiting IgE anisotropy and slightly prolongs the rotational correlation time. Aggregation of FcεRI by antigen thus produces the expected effects on the rotational motions of the receptor (*46, 55*).

Restriction of FcεRI-IgE motion by anti-IgE has also been reported (*45, 47*). In our hands, the main effect of anti-IgE treatment is to increase the IgE initial anisotropy, while further clustering with anti-IgG increases both the initial and limiting anisotropies. By contrast, it is reassuring that substantial effects of MAFA clustering on FcεRI rotation (or lateral diffusion) are *not* observed. Since unperturbed FcεRI are generally agreed to be monomeric (*56*) and since they outnumber MAFA by about 20 to 1 in the membrane, it is difficult to envision how FcεRI motions could be substantially affected by clustering the relatively few MAFA molecules.

Lateral diffusion of FcεRI and its ligand-induced aggregates has been previously examined using fluorescence photobleaching recovery, first by Metzger and Schlessinger (*57, 58*) and subsequently by other investigators (*59*−*61*), as well as by other techniques (*62*). Our values for the IgE lateral diffusion coefficient and mobile fraction resemble those first reported by Schlessinger et al. (*58*). Antigen treatment of IgE-binding FcεRI seems primarily to affect the receptor diffusion coefficient rather than its mobile fraction. The Saffmann−Delbrück treatment of diffusion in membranes shows that *lateral* diffusion depends only on the logarithm of the size of the diffusing species (*28*). This logarithmic dependence suggests why simple aggregation of a membrane protein should affect only its diffusion coefficient (*34*). Moreover, we showed that DNP_{11}-BSA treatment reduced the diffusion coefficient of receptor-bound IgE from 3.9×10^{-10} cm^2 s^{-1} on untreated cells to 2.8×10^{-10} cm^2 s^{-1} after DNP_{11}-BSA treatment. This actually demonstrates substantial aggregation. These numbers, together with the membrane parameters employed by Peters and Cherry (*49*), imply that the aggregates formed involved at least 36 receptors. Naturally, such large aggregates would be expected to appear immobile rotationally, and, indeed, the effect of antigen treatment was to increase the FcεRI limiting anisotropy while leaving the rotational correlation time essentially unchanged (Table 2).

The other major objective of the experimentation is comparison of MAFA rotation as modulated by monovalent or oligovalent ligands. In view of the experimental difficulties in monitoring the low signals produced by the Er-G63 Fab, it can only be said that these results are *consistent* with association of MAFA with FcϵRI on unperturbed cells. Other types of experimental data are needed to further pursue this matter. Still, membrane dynamic data *do* permit resolution of a related question, namely, whether MAFA, not itself specifically clustered, is nonetheless associated with *clustered* FcϵRI. Table 2 shows effects of antigen or anti-IgE clustering of FcϵRI on MAFA-bound G63 Fab rotation. Both means of aggregating FcϵRI increase the limiting and initial anisotropies and rotational correlation time of G63 Fab. These data were obtained by comparing similarly treated and control samples in multiple experiments. We have already indicated that each individual effect of FcϵRI clustering is at the verge of statistical significance. However, when both treatments' effects on initial and limiting anisotropies are considered together, the probability that MAFA motion is unaffected by these treatments becomes vanishingly small. Moreover, MAFA rotational correlation times, though not analyzed statistically, also increase upon FcϵRI clustering. Thus, rotation measurements clearly suggest *either* that aggregating FcϵRI induces interactions between the receptor and G63 Fab-binding MAFA *or* that these interactions already exist with unclustered FcϵRI. In either case, the restriction of MAFA rotation caused by FcϵRI clustering would directly reflect the lower mobility of aggregated FcϵRI. By contrast, the rotational diffusion parameters of MAFA when binding intact mAb G63 are virtually identical in the presence and absence of FcϵRI clustering.

The data in Table 4, particularly the absence of a larger difference between the rotational correlation times of mAb- and Fab-binding MAFA, are challenging to interpret. The intrinsic problem is weak luminescence signals, a consequence of MAFA's low surface expression. These signals cause large uncertainties in measured rotational correlation times and anisotropies. Nonetheless, one factor possibly limiting rotational differences between mAb- and Fab-labeled samples can be easily suggested. Only a fraction of MAFA may be associated with FcϵRI [Schweitzer-Stenner et al. (*27*) estimated 60%]; and, given MAFA's small size, these nonassociated molecules would rotate quite rapidly. If an mAb molecule were to cross-link such an isolated MAFA with an FcϵRI-associated MAFA, the complex would move in much the same way as the receptor-associated species binding an Fab. In such a circumstance, mAb-labeled samples would be expected to rotate somewhat slower than Fab-labeled ones, but not as much as 2-fold slower. This is what is observed. We also noted that the initial and limiting anisotropy values and rotational correlation times of mAb-labeled samples were not greatly changed by DNP_{11}-BSA treatment and, in fact, resembled those of Fab-labeled samples *after* DNP_{11}-BSA treatment. This appears grossly consistent with previous results showing that the efficiency of energy transfer between MAFA-bound G63 mAb and FcϵRI-bound IgE is not increased by FcϵRI clustering (*26*). However, an actual mechanism by which mAb binding to two MAFA molecules could have the same effects on rotational mobility as formation by DNP_{11}-BSA of large FcϵRI aggregates involving MAFA is difficult to envision.

Further support for the interaction of MAFA with (at least) aggregated FcϵRI comes from the lateral diffusion measurements of MAFA. Figure 3 clearly shows a slowing of MAFA's lateral diffusion upon antigen treatment, though the effect is not nearly as pronounced at that induced by direct aggregation of MAFA using G63 Fab and anti-IgG. Although steric factors resulting from FcϵRI clustering could affect MAFA diffusion indirectly, such behavior would be observed if all MAFA molecules were intrinsically associated with both isolated and aggregated FcϵRI. In such a case, both MAFA lateral and rotational diffusion should consistently resemble those of its associated FcϵRI so that clustering the receptor should similarly affect both FcϵRI and MAFA dynamics. Certainly, the *effects* of FcϵRI clustering appear similar, as do most of the dynamic parameters of the two molecules. The discrepancy in the mobile fractions of MAFA and FcϵRI may simply arise from the sensitivity of interference fringe photobleaching measurements to the accuracy of correction for cellular background autofluorescence (*42*).

A final issue concerns the possible involvement of the Fcγ domain of intact mAb G63 in inhibition of the 2H3 cell secretory responses. In replicate experiments on comparably handled samples, we found that intact mAb G63 exhibits higher anisotropies than G63 $F(ab')_2$ and that these overall differences are highly significant. The mAb G63 is of the IgG_1 subtype (*4*), which has the highest affinity for the type IIB Fcγ receptor (FcγRIIB). This receptor is known to inhibit activation signals produced by ITAM-containing receptors upon co-clustering with ITIM-containing receptors (*63*). Thus, it is attractive to suppose that inhibition of the secretory response by mAb G63 might be potentiated by the interaction of its Fcγ domain with other ITIM-containing receptors also expressed on 2H3 cells, as rotational motion measurements suggest. Indeed a slight yet significantly higher inhibition of the FcϵRI-induced secretory response has been observed when intact G63 mAb is used compared with its $F(ab')_2$ fragment (A. Licht and I. Pecht, unpublished results).

Taken together, the above results support a model that is currently emerging for MAFA's inhibitory action: MAFA clustering causes a transient increase in phosphorylation of its own ITIM tyrosyl residue. The tyrosyl-phosphorylated ITIM recruits phosphatases, primarily the SH2 domain-containing phosphatase SHIP, which deplete the membrane levels of signaling phosphatidyinositol phosphates produced upon FcϵRI clustering. The results presented here indicating association of MAFA with the FcϵRI further support this model since the spacial proximity of MAFA to the FcϵRI signaling complex would rationalize the efficacy of MAFA's action.

ACKNOWLEDGMENT

We are most grateful to Mr. Arieh Licht for preparation of mAb G63 and other reagents used in these studies.

REFERENCES

1. DeLisi, C. (1980) *Q. Rev. Biophys. 13*, 201−230.
2. Ishizaka, T., Chang, T. H., Taggart, M., and Ishizaka, K. (1977) *J. Immunol. 119*, 1589−1596.
3. Barsumian, E. L., Isersky, C., Petrino, M. G., and Siraganian, R. P. (1981) *Eur. J. Immunol. 11*, 317−323.
4. Soto, E. O., and Pecht, I. (1988) *J. Immunol. 141*, 4324−4332.

5. Schwartz, L. (1994) *Curr. Opin. Immunol. 6*, 91−97.
6. Ortega, E., Hazan, B., Zor, U., and Pecht, I. (1989) *Eur. J. Immunol. 19*, 2251−2256.
7. Bradding, P., Feather, I., Wilson, S., Bardin, P., Heusser, C., Holgate, S., and Howarth, P. (1993) *J. Immunol. 151*, 3853−3865.
8. Galli, S. J., Gordon, J. R., and Wershil, B. K. (1991) *Curr. Opin. Immunol. 3*, 865−872.
9. Eiseman, E., and Bolen, J. B. (1992) *Nature 355*, 78−80.
10. Scharenberg, A. M., Lin, S., Cuenod, B., Yamamura, H., and Kinet, J. (1995) *EMBO J. 14*, 3385−3394.
11. Benhamou, M., Gutkind, J. S., Robbins, K. C., and Siraganian, R. P. (1990) *Proc. Natl. Acad. Sci. U.S.A. 87*, 5327−5330.
12. Beaven, M., Moore, J., Smith, G., Hesketh, T., and Metcalfe, J. (1984) *J. Biol. Chem. 259*, 7137−7142.
13. Sagi-Eisenberg, R., Lieman, H., and Pecht, I. (1985) *Nature 313*, 59−60.
14. Guo, N., Her, G., Reinhold, V., Brennan, M., Siraganian, R., and Ginsburg, V. (1989) *J. Biol. Chem. 264*, 13267−13272.
15. Ortega, E., Licht, A., Biener, Y., and Pecht, I. (1990) *Mol. Immunol. 27*, 1269−1277.
16. Stephan, V., Guo, N., Ginsburg, V., and Siraganian, R. (1991) *J. Immunol. 146*, 4271−4277.
17. Kitani, S., Berenstein, E., Mergenhagen, S., Tempst, P., and Siraganian, R. (1991) *J. Biol. Chem. 266*, 1903−1909.
18. Hamawy, M., Oliver, C., and Siriganian, R. (1992) *J. Immunol. 148*, 524−531.
19. Ortega, E., and Pecht, I. (1988) *J. Immunol. 141*, 4324−4332.
20. Guthmann, M. D., Tal, M., and Petch, I. (1995) *Int. Arch. Allergy Immunol. 107*, 82−86.
21. Guthmann, M. D., Tal, M., and Pecht, I. (1995) *Proc. Natl. Acad. Sci. U.S.A. 92*, 9397−9401.
22. Binsack, R., and Pecht, I. (1997) *Eur. J. Immunol. 27*, 2557−2561.
23. Rong, X., and Pecht, I. (1996) *Immunol. Lett. 54*, 105−108.
24. Kubitscheck, U., Kircheis, M., Schweitzer-Stenner, R., Dreybrodt, W., Jovin, T. M., and Pecht, I. (1991) *Biophys. J. 60*, 307−318.
25. Field, K. A., Holowka, D., and Baird, B. (1995) *Proc. Natl. Acad. Sci. U.S.A. 92*, 9201−9205.
26. Jurgens, L., Arndt-Jovin, D., Pecht, I., and Jovin, T. M. (1996) *Eur. J. Immunol. 26*, 84−91.
27. Schweitzer-Stenner, R., Engelke, M., Licht, A., and Pecht, I. (1999) *Immunol. Lett. 68 (1999)*, 71−78.
28. Saffman, P. G., and Delbrück, M. (1975) *Proc. Natl. Acad. Sci. U.S.A. 72*, 3111−3113.
29. Baniyash, M., and Eshhar, Z. (1984) *Eur. J. Immunol. 14*, 799−807.
30. Carsten, M. E., and Eisen, H. N. (1953) *J. Am. Chem. Soc. 75*, 4451−4456.
31. Johnson, G. D., and Holborow, E. J. (1986) in *Handbook of Experimental Immunology* (Weir, D. M., Ed.) pp 28.1−28.21, Blackwell Scientific Publications, Boston.
32. Peng, H., and Barisas, B. G. (1997) *J. Fluoresc. 7*, 139−145.
33. Johnson, P., and Garland, P. B. (1981) *FEBS Lett. 132*, 252−256.
34. Barisas, B. G., Wade, W. W., Jovin, T. M., Arndt-Jovin, D., and Roess, D. A. (1999) *Mol. Immunol. 36*, 701−708.
35. Philpott, C. J., Rahman, N. A., Kenny, N., Barisas, B. G., and Roess, D. A. (1995) *Biol. Reprod. 53*, 645−650.
36. Herman, J. R., Londo, T. R., Rahman, N. A., and Barisas, B. G. (1992) *Rev. Sci. Instrum. 63*, 5454−5458.
37. Austin, R. H., Chan, S. S., and Jovin, T. M. (1979) *Proc. Natl. Acad. Sci. U.S.A. 76*, 5650−5654.
38. Bevington, P. R. (1969) *Data reduction and error analysis for the physical sciences*, McGraw-Hill Book Co., New York.
39. Rahman, N. A., Pecht, I., Roess, D. A., and Barisas, B. G. (1992) *Biophys. J. 161*, 334−361.
40. Student (1907) *Biometrika 5*, 351−360.
41. Sokal, R. P., and Rohlf, F. J. (1969) *Introduction to biostatics*, 1st ed., W. H. Freeman and Co., San Francisco.
42. Munnelly, H. M., Roess, D. A., Wade, W. F., and Barisas, B. G. (1998) *Biophys. J. 75*, 1131−1138.
43. Marquardt, D. W. (1963) *J. Soc. Ind. Appl. Math. 11*, 431−441.
44. Bocek, P., Jr., Draberova, L., Draber, P., and Pecht, I. (1995) *Eur. J. Immunol. 25*, 2948−2955.
45. Zidovetzki, R., Bartholdi, M., Arndt-Jovin, D., and Jovin, T. (1986) *Biochemistry 25*, 4397−4401.
46. Pecht, I., Ortega, E., and Jovin, T. M. (1991) *Biochemistry 30*, 3450−3458.
47. Myers, J. N., Holowka, D., and Baird, B. (1992) *Biochemistry 31*, 567−575.
48. Soto, E. O. (1990) Ph.D. Thesis, Weizmann Institute of Science, Rehovot, Israel.
49. Peters, R., and Cherry, R. J. (1982) *Proc. Natl. Acad. Sci. U.S.A. 79*, 4317−4321.
50. Palczewski, K., Kumasaka, T., Hori, T., Behnke, C., Motoshima, H., Fox, B., Le Trong, I., Teller, D., Okada, T., Stenkamp, R., Yamamot, M., and Miyano, M. (2000) *Science 289*, 739−745.
51. Munnelly, H. M., Brady, C. J., Hagen, G. M., Wade, W. F., Roess, D. A., and Barisas, B. G. (2000) *Int. Immunol. 12*, 1319−1328.
52. Field, K. A., Holowka, D., and Baird, B. (1997) *J. Biol. Chem. 272*, 4276−4280.
53. Cantor, C. R., and Schimmel, P. R. (1980) in *Biophysical Chemistry II*, p 441, W. H. Freeman, San Francisco.
54. DeLisi, C., and Perelson, A. (1976) *J. Theor. Biol. 62*, 159−210.
55. Rahman, N. A., Pecht, I., Roess, D. A., and Barisas, B. G. (1992) *Biophys. J. 61*, 334−346.
56. Kubitscheck, U., Schweitzer-Stenner, R., Arndt-Jovin, D. J., Jovin, T. M., and Pecht, I. (1993) *Biophys. J. 64*, 110−120.
57. Mendoza, G., and Metzger, H. (1976) *Nature 264*, 548−550.
58. Schlessinger, J., Webb, W. W., Elson, E. L., and Metzger, H. (1976) *Nature 264*, 550−552.
59. Menon, A. K., Holowka, D., Webb, W. W., and Baird, B. (1986) *J. Cell Biol. 102*, 534−540.
60. Menon, A., Holowka, D., Webb, W., and Baird, B. (1986) *J. Cell Biol. 102*, 541−550.
61. Goldstein, B., Posner, R. G., Torney, D. C., Erickson, J., Holowka, D., and Baird, B. (1989) *Biophys. J. 56*, 955−966.
62. McCloskey, M. A., Liu, Z.-Y., and Poo, M.-M. (1984) *J. Cell Biol. 99*, 778−787.
63. Daeron, M. (1997) *Annu. Rev. Immunol. 15*, 203−234.

BI011566I